ARMY RESEARCH LABORATORY

Deformation Behavior of 93W-5Ni-2Fe at Different Rates of Compression Loading and Temperatures

by Tusit Weerasooriya

ARL-TR-1719 July 1998

The findings in this report are not to be construed as an official Department of the Army position unless so designated by other authorized documents.

Citation of manufacturer's or trade names does not constitute an official endorsement or approval of the use thereof.

Destroy this report when it is no longer needed. Do not return it to the originator.

Army Research Laboratory
Aberdeen Proving Ground, MD 21005-5069

ARL-TR-1719 **July 1998**

Deformation Behavior of 93W-5Ni-2Fe at Different Rates of Compression Loading and Temperatures

Tusit Weerasooriya
Weapons and Materials Research Directorate, ARL

Abstract

Low (0.0001 to 0.1 s^{-1}) and high (9,000 s^{-1} average) strain-rate uniaxial compression experiments were performed on a tungsten heavy alloy (WHA) at room temperature; high-rate experiments were conducted using the Compression Split-Hopkinson Bar apparatus. In addition, high-temperature tests at 423, 573, and 732 K were conducted at 0.1 s^{-1} strain-rate. The deformation and failure behaviors of this alloy under compression loading were examined in this report in comparison to the previous torsional work on the same alloy. The deformation behaviors of WHA were modeled using modified Johnson-Cook (JC) and Power-Law (PL) models. A functional form based on microphysics was proposed to represent the temperature part of these models. The model constants were determined from test data at both room and other temperatures. The constants for WHA alloy for these two models are summarized in this report.

Acknowledgment

The author gratefully acknowledges the assistance of Paul Moy in conducting the tests.

INTENTIONALLY LEFT BLANK

Table of Contents

INTENTIONALLY LEFT BLANK

List of Figures

INTENTIONALLY LEFT BLANK

List of Tables

INTENTIONALLY LEFT BLANK

1. Introduction

Tungsten heavy alloys (WHA) are used in many applications, both at low- and high-rates of loading, because of their physical and mechanical properties such as high density, high strength, good ductility, and good corrosion resistance [1–3]. In general, these mechanical properties are obtained at slow loading rates. Since these alloys are mostly used as penetrators, which are subjected to dynamic or impact loading conditions, it is essential to evaluate their mechanical properties and deformation/failure behavior under high strain-rate loading.

In this type of application, the penetrator material is subjected to a multiaxial stress state at high-rate loading before failure. To study the effect of stress state on the high-rate deformation/failure behavior of WHAs, it is necessary to systematically obtain experimental deformation/failure characteristics, including micromechanisms, at different types of high-rate loading such as compression, tension, pure shear (torsion), and shear under pressure. In our previous work at the U.S. Army Research Laboratory (ARL), the deformation/failure behavior of a WHA, 93W-5Ni-2Fe swaged to 17%, has been studied in detail under torsional loading at different strain-rates including high-rates [4]. Also, shearing under pressure [5] and torsion under axial compression [6] experiments have been reported for the same WHA. The uniaxial compression work at different strain-rates reported in this paper provides the deformation/failure behavior at another stress state of loading for the same WHA.

To develop better materials for penetrators, the knowledge of the influence of microstructure on the deformation and failure process during high-rates is essential. Most of the reported work under high loading rates is directed to obtain the rate sensitivity of the stress-strain behavior. Studies that are conducted at high-rates, in addition to providing macroscopic stress-strain behavior, should also provide microstructural information to facilitate the alloy developer.

This work is a continuation of the research that was undertaken to study and understand in detail the deformation/failure behavior of a standard penetrator WHA (93W-5Ni-2Fe) under quasi-static to high strain-rate loading conditions. Previously reported work covers the aspect of deformation/failure behavior under torsional loading on this material[4, 7, 8]. This material was chosen as the base-line reference material for future studies on other WHAs with different processing and microstructural features and constituents. In this study, uniaxial compression

behavior of the WHA is obtained as a function of strain-rate and temperature. After the tests, microstructural analysis is performed to identify any failures and mechanisms associated with failure. Deformation/failure behavior and failure mechanisms under torsion loading from our previous work is compared with that from compression experiments from this paper.

In addition, in this paper, the experimentally generated isothermal behavior of the material is represented by two thermo-viscoplastic phenomenological models: the Johnson-Cook (JC) model, which is available in most of the computer codes, and the Power-Law (PL) model, which is frequently used by the material scientists. The part of these models that contains the temperature effect is evaluated with the temperature data and modified to provide a more realistic and representative functional form.

2. Experiments

2.1 Material.

The 93%W alloy for the this study was obtained from Teledyne. The manufacturer provided chemical composition and the mechanical properties of this alloy are listed in Table 1.

Table 1. Chemical Composition and Mechanical Properties From Manufacturer

Alloy	Chemical Composition			Physical and Mechanical Properties			
	W (%)	Ni (%)	Fe (%)	Density (g/cm^3)	Hardness (R_c)	UTS (MPa)	Elongation (%)
93W-7Ni-3Fe	92.85	4.9	2.25	17.70	39.5	1,103	13

According to the 93% WHA processing information obtained from Teledyne, initially, a mixture of W, Ni, and Fe powder was isostatically pressed to 207 MPa (30,000 psi) in a drybag press. The pressed material was then sintered in a hydrogen atmosphere in a molybdenum furnace at about 1,520° C. The hydrogen atmosphere was used to reduce the surface oxides of the powder. The sintered material was vacuum-annealed at about 1,000° C for 10 hr to remove the absorbed hydrogen. The annealed material was heated in an inert gas atmosphere to about 1,100° C, soaked for about an hour, and, finally, water-quenched to give better dynamic impact properties. The bars were then machined and swaged to 17%.

Figure 1 shows the microstructure of this alloy taken in the longitudinal direction. Microstructure in the transverse direction is similar to the one in the longitudinal direction. Swaging to 17% does not seem to affect the microstructure of the alloy. As shown in the figure, the microstructure consists of two phases: nearly pure W spherical grains of body-centered cubic (bcc) crystal structure and W-Ni-Fe matrix of face-centered cubic (fcc) crystal structure. Matrix material provides the ductility for the W alloy with these brittle W grains. The size of the W grains is approximately 27 μm and is mostly surrounded by a thin layer of matrix material. However, some W grains are in contact with adjacent W grains.

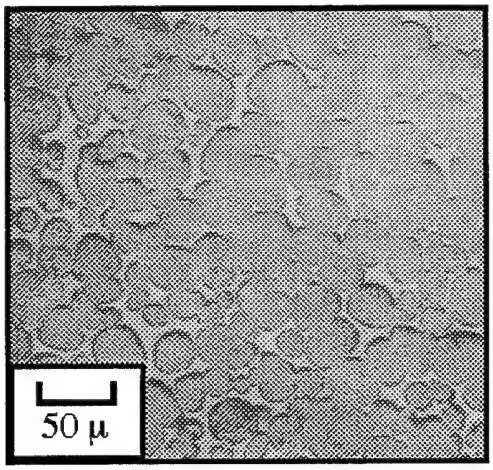

Figure 1. Microstructure of 93W-5Ni-2Fe WHA Swaged to 17%.

2.2 Specimen Geometry.

The geometry of the compression specimen is shown in Figure 2. The specimen is a cylinder with a 6.350-mm diameter and 3.175-mm gauge length. On the two loading surfaces of the specimen, concentric grooves are machined, as shown in the figure. The purpose of these grooves is to hold the lubricant as long as possible while the specimen is deforming. These grooves enable us to reduce the barreling of the specimen to a negligible amount, thus maintaining the cylindrical geometry up to a large strain. The same specimen geometry was used for all the testing: slow- and high-rate, as well as high-temperature, testing.

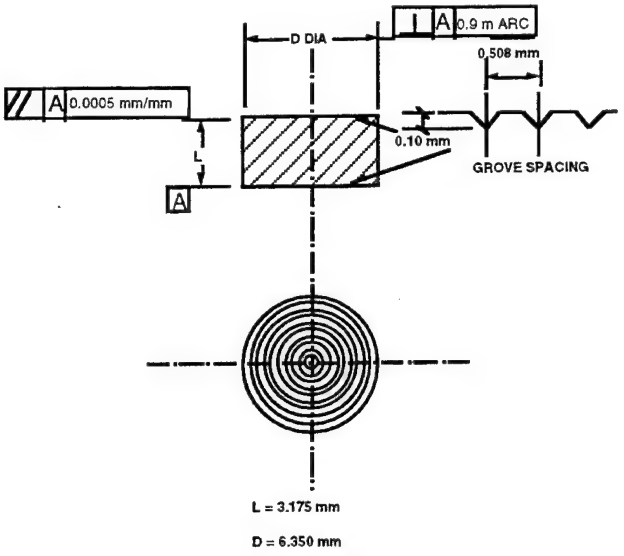

Figure 2. Specimen Geometry.

2.3 Compression Experiments.

2.3.1 High-Rate Tests.

The high-rate compression tests were conducted using a compression Split-Hopkinson Bar. A schematic of the compression Hopkinson Bar at ARL is given in Figure 3. A wave interaction diagram for the Hopkinson Bar is also given in this figure. It consists of two bars (input and output bars) with a 25.4-mm diameter and 1,524-mm length and made of Maraging 350 steel. Each bar is held by six bronze bearings, which are aligned accurately with a laser beam. A detailed description of the alignment procedure is given elsewhere [9]. Cylindrical compression specimen is held between the two bars. Silicone grease lubricant is applied on the grooved loading surfaces of the specimen. High-rate compression loading is applied on the specimen by impacting a striker bar on the input bar. The 25.4-mm-diameter and 400-mm-length striker bar, made out of Maraging 350 steel, is propelled from a gas gun at the nonspecimen end of the input bar. The duration of the resulted compression pulse in the input bar from this impact is twice the time it takes the stress pulse to travel from one end to the other end of the striker. The incident compression stress pulse travels toward the specimen after the impact; at the specimen, part of the pulse transmits through the specimen to the output bar and the remainder reflects back to the input bar. The incident, reflected, and transmitted pulses are monitored from the strain gauges mounted at the midspan of the input and output bars. At each gauge location on the bars, two strain gauges are mounted at diametrically opposite locations on the bar and connected in series

to cancel any strain components from bending of the bar. The signals from the gauge stations are fed into 1-MHz-bandwidth high-speed strain-gauge bridge amplifiers. Output from the amplifiers is captured by a 500-kHz Nicolet digital oscilloscope and then transferred to a personal computer for further analysis of the data. The stress, strain, and strain-rate as a function of time can be inferred from this data as discussed in the next section.

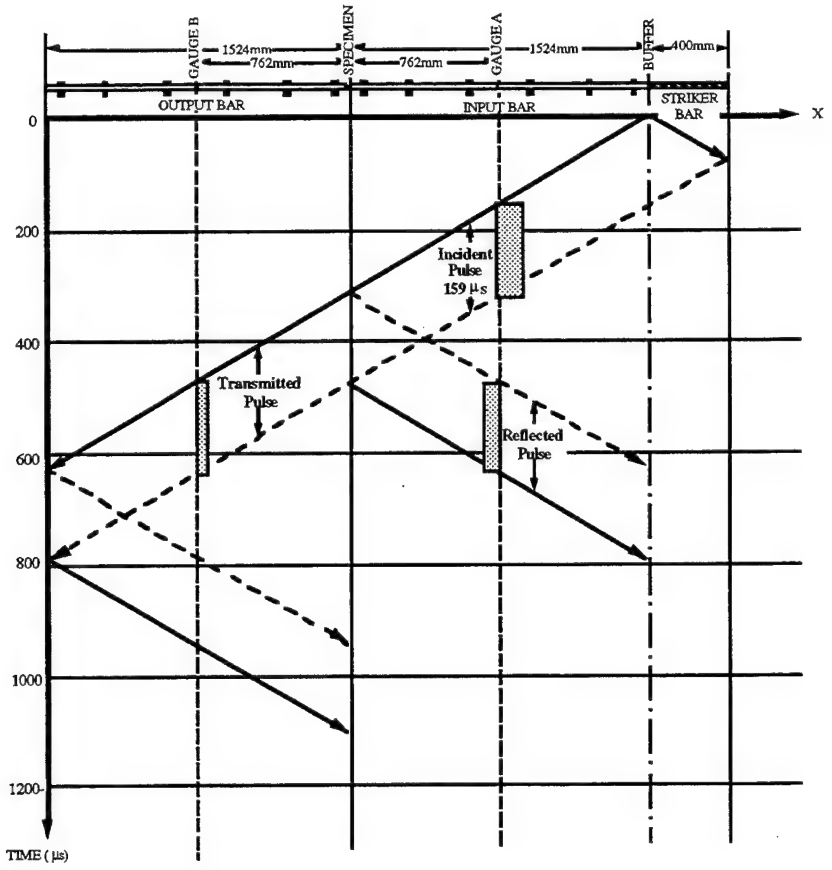

Figure 3. Schematic of the Compression Split-Hopkinson Bar With the Lagrangian (x-t) Diagram.

The magnitude of stress, strain, and strain-rate of the specimen can be computed using Kolsky analysis from the measured strain records of the input and output bar gauges [10, 11]. Strain-rate at the specimen ($\dot{\varepsilon}_s$) is given by

$$\dot{\varepsilon}_s = \frac{-2C_l}{L_s}\varepsilon_r, \tag{1}$$

where C_l is the longitudinal sound velocity in the input and output bars, L_s is the gauge length of the specimen, and ε_r is the reflected strain in the input bar. Stress in the specimen σ_s is given by

$$\sigma_s = \frac{EA_b}{A_s}\varepsilon_t, \tag{2}$$

where E is the Young's modulus of the material of the bars, A_S is the cross-sectional area of the specimen, A_b is the cross-sectional area of the bars, and ε_t is the transmitted strain in the output bar. By integrating equation (1), strain in the specimen can be obtained by

$$\varepsilon_s = \int_0^t \frac{-2C_1}{L_s}\varepsilon_r \cdot dt. \tag{3}$$

A computer program based on equations (1)-(3) similar to the one in Weerasooriya [9] was used to obtain the dynamic stress-strain and strain-rate–time relationship.

2.3.2 Slow-Rate Tests.

Slow rate (0.1 and 0.0001 s^{-1}) compression tests were conducted using a servocontrolled Instron hydraulic test machine. True strain-rate was held constant during testing, while the displacement and load were monitored. This was accomplished by feeding an exponentially decaying reference input voltage to the testing machine via a function generator controlled by a computer. The required exponential waveform is set up in the function generator by a computer program. To correct the measured displacement data, compliance of the machine was also measured without any specimens.

In addition, to obtain the effect of temperature on the deformation, high-temperature uniaxial compression tests were conducted at a true strain-rate of 0.1 s^{-1} using the servocontrolled Instron hydraulic testing machine. The specimen was heated to the test temperature by radiant heating from a clam shell oven with heating lamps. Test temperature was controlled to ±1° C from the required temperature. To obtain the effect of temperature, tests were conducted at three high-temperatures: 423, 573, and 732 K.

3. Results and Discussion

3.1 Stress-Strain Behavior.

3.1.1 As a Function of Strain-Rate at 293 K.

Uniaxial stress compression behaviors at strain-rates 0.0001, 0.1, and 9,000 s^{-1} above experiments are shown in Figure 4 for this material. At the lower rates (0.0001 and 0.1 s^{-1}), this WHA work-hardens as the strain is increased. Work-hardening rates from both strain-rates is approximately equal. At the higher rate, 9,000 s^{-1}, material softens with strain, indicating that thermal softening dominates over strain and strain-rate hardening. Softening starts just after yielding of the material. Yield stress of the material is highly strain-rate sensitive and increases with strain-rate. Rate sensitivity of this material is discussed in detail in a later section of this report.

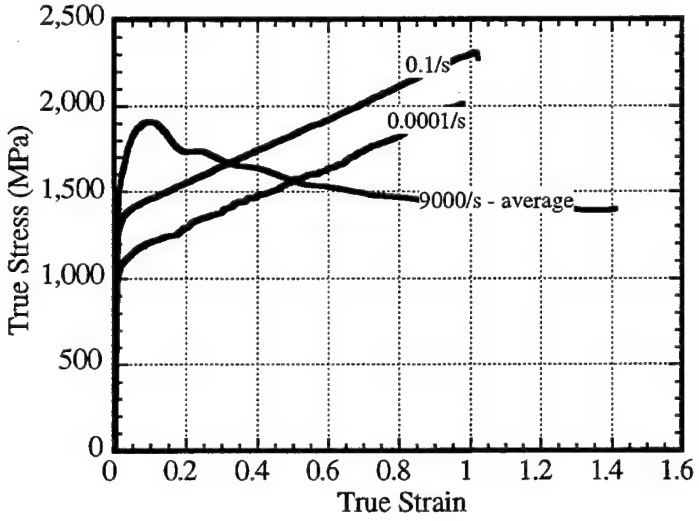

Figure 4. Stress-Strain Behavior as a Function of Strain-Rate at 293 K.

3.1.2 As a Function of Temperature at 0.1 s^{-1} Strain-Rate.

Stress-strain behaviors from the high-temperature tests at 0.1 s^{-1} strain-rate at different temperatures are given in Figure 5. Also in this figure, room-temperature (293 K) stress-strain behaviors are plotted with the high-temperature results. From these results, in general, as the temperature is increased, the flow stress decreases at a given strain except for the lower strains (strains less than 0.02) for the test at 573 K.

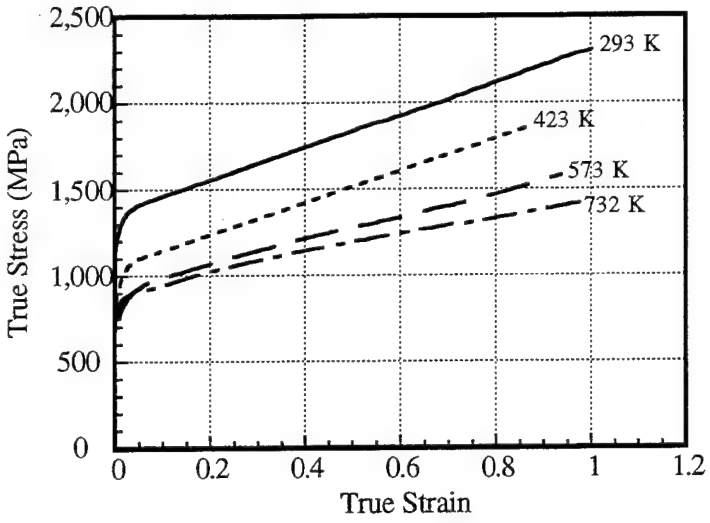

Figure 5. Stress-Strain Behavior as a Function of Temperature at 0.1 s^{-1} Strain-Rate.

3.2 Comparison With Torsional Deformation/Failure Behavior.

Shear stress-shear strain behavior as a function of strain-rate for this material from torsion experiments was reported in an earlier publication [4]. In this section, these shear data are compared with the experimental data obtained from the compression tests.

3.2.1 Representation of Deformation Data by von Mises Effective Stress-Strain.

For most materials, it has been reported that, for small strains, the torsion and compression data can be correlated by representing stresses and strains with von Mises effective stress ($\bar{\sigma} = \sigma$ or $\sqrt{3}\tau$) and strain ($\bar{\varepsilon} = \varepsilon$ or $\gamma/\sqrt{3}$), respectively. Here, σ and ε represent the stresses and strains from compression tests and τ and γ represent shear stresses and strains from torsion tests. But, at large strains, this correlation is not applicable due to the crystallographic anisotropy that develops in the material [12, 13]. At large strains, different anisotropic textures form under torsion and compression loading in single-phase materials. Previous results from other materials, such as copper, show that the torsion stress-strain curve lies below both the tensile and compressive curves at large strains when they are plotted as effective stress-strain plots.

The effective stress-strain plots from the compression and torsion tests on WHA (two-phase composite) at different strain-rates are shown in Figure 6. Because the material softens after the yield due to adiabatic heating at higher rates, high-rate data after the yield cannot be used for the

comparison of the compression data with the torsional flow behavior. For lower rate (0.1 and 0.0001 s^{-1}) stress-strain data, the compression stress-strain curves lie above the torsion stress-strain curves for the total range of strains, including lower strains. Though the deformation after the yield cannot be collapsed to a single curve, yield stresses at all rates, including the high-rate yield stresses obtained from extrapolated data, can be correlated with the effective stress representation within the experimental scatter.

At lower rates, the rate of work-hardening for torsion tests is much lower than that from compression tests. In both types of loading at high-rates, thermal softening dominates over combined strain and strain-rate hardening, showing a decreasing effective flow stress with increasing strain.

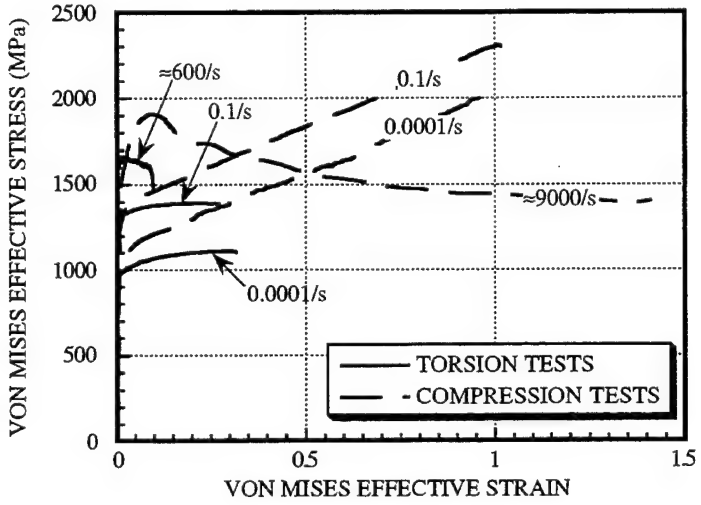

Figure 6. Comparison of Compression and Torsion Stress-Strain Data When Plotted as von Mises Effective Stress vs. Strain. Torsion Stress-Strain Data Are From Weerasooriya and Beaulieu [4].

3.2.2 Comparison of Maximum Shear Strains and Final Microstructures.

Both compression and torsion data are plotted in Figure 7 as maximum shear stress vs. maximum shear strain plots. Maximum shear stress and strain are chosen because the material would fail under shear. In our compression experiments, the maximum shear strains that were reached were not high enough for the failure. But in torsion experiments, specimens failed in the direction of the maximum shear for all the strain-rates.

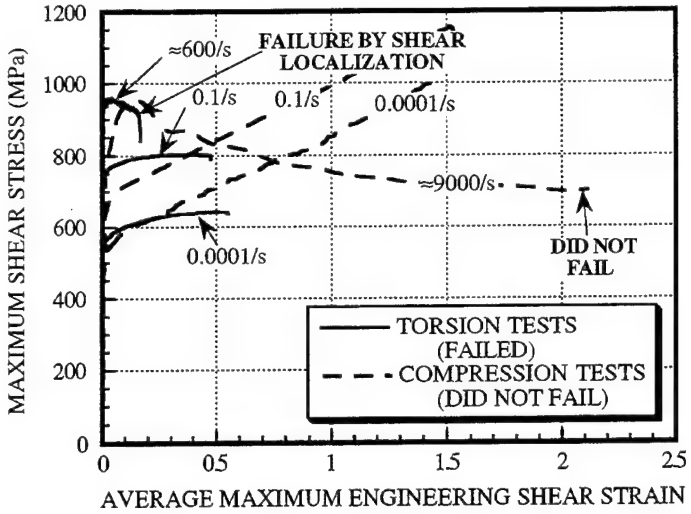

Figure 7. Comparison of Compression and Torsion Stress-Strain Data When Plotted as Maximum Shear Stress vs. Maximum Shear Strain. Torsion Stress-Strain Data Are From Weerasooriya and Beaulieu [4]. None of the Compression Specimens Failed During the Loading. Torsion Specimens Failed at a Much Smaller Shear Strain Than the Maximum Shear Strain Reached in Compression Tests, but Only the High-Rate Torsion Tests Failed by Shear Localization.

At lower rates of loading, torsion specimens failed along the maximum shear direction after going through a uniform deformation. In contrast, in high-rate torsion tests, the specimens failed by shear localization along the direction of maximum shear strain (see Figure 8a). In torsion tests, the maximum shear plane lies approximately parallel to the direction of the applied shear. Cavities were present in the highly deformed localized shear area, at the matrix-W grain interface, where the major axis of the elliptically deformed W grains meets the matrix. Failure shear strain was 0.18. But, in high-rate compression tests, specimens did not fail up to a maximum shear strain of 2.2 (see Figure 8b). All W grains have flattened in the loading direction. Their are no signs of shear localization in the specimen. This observation contradicts what was observed by Lankford, Bose, and Couqe [14] for most of WHAs they tested under compression loading. They observed failure by shear localization at lower strains along the maximum shear direction, which laid 45° inclined to the loading axis in the uniaxial compression tests. But, in their experiments, specimens barreled due to the friction at the loading surfaces during the testing. During barreling, stress state is not uniform and not uniaxial. As shown by Mescall, Papirno, and McLaughlin [15], a complex nonuniform triaxial state of stress, including tensile stresses, exists in the specimen. Even though the failure mechanisms are identified in

their tests, we cannot obtain the complete state of the actual stress and strain conditions that initiates these localized adiabatic shear bands from macroscopic measurements.

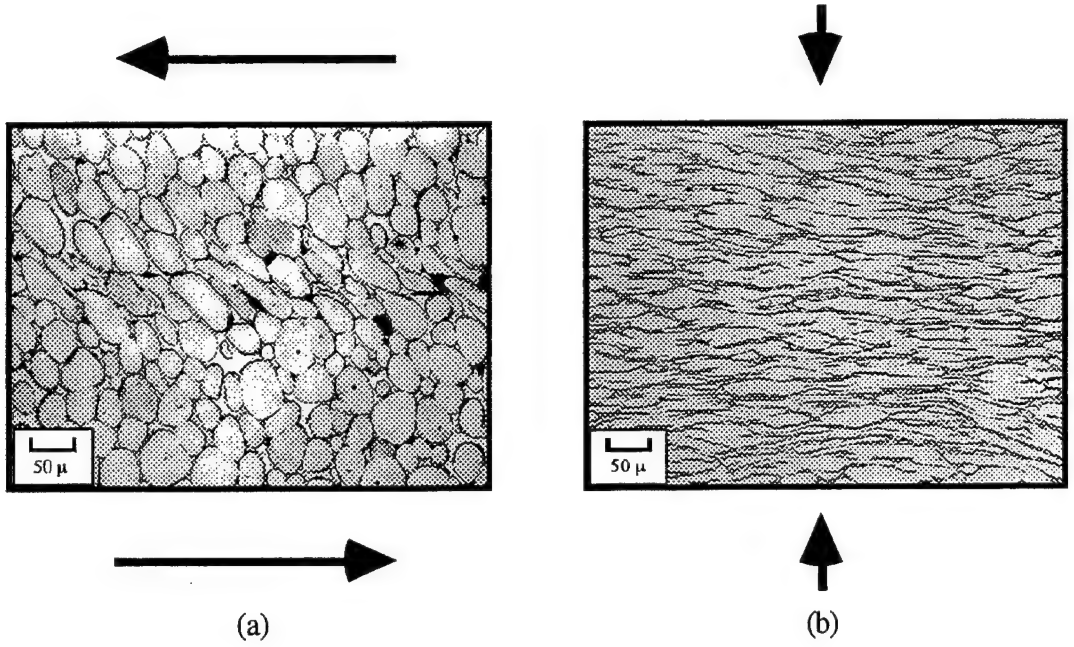

Figure 8. Optical Micrographs of the Specimens (a) at the End of the High-Rate Torsional Loading From Weerasooriya and Beaulieu [4] (Maximum Shear Strain = 0.18) and (b) at the End of the High-Rate Compression Loading (Maximum Shear Strain = 2.2). Only the Specimens Subjected to High-Rate Torsional Loading Show Shear Localization.

Though our compression experiments specimens did not fail by shear even up to a shear strain of 2.2, Zhou, Clifton, and Needleman [5] observed the failure of this WHA by shear localized instability in their pressure-shear experiments at a maximum shear strain of 1.4 under a 10-GPa high hydrostatic compression. Shear strain-rate of these experiments was much higher and close to a 650,000 s^{-1} strain-rate in comparison to 9,000 s^{-1} strain-rate in our compression experiments. Specimens failed by pure thermal instability initiated localization compared to cavity-assisted localization in pure shear (torsion). Also, it is important to stress that their experiments were conducted with very thin samples of 57 to 89 μm (approximately three to four W grains across the thickness).

3.3 Modeling the Deformation Behavior.

Model constants of the two models discussed in this section have been obtained from room-temperature stress-strain data at 0.0001 and 0.1 s^{-1} strain-rates, and 0.1 s^{-1} strain-rate stress-strain data at 423, 573, and 732 K.

3.3.1 Effect of Strain-Rate.

In Figure 9(a) and (b), yield stress is shown as a function of strain-rate in semi-log and log-log plots, respectively. This material is extremely strain-rate sensitive at the room temperature. Linear correlation from both log-log (correlation coefficient, R = 0.99727) and semi-log (R = 0.9892) representations are reasonable. A similar possibility of dual correlation was also observed from the torsion experimental data for this alloy [7]. This observation suggests the feasibility of using either a logarithmic law or a PL for modeling the flow stress behavior for rate effects for this material. For behavior at different rates of straining, researchers have proposed both exponential [16–19] and PL-type [20, 21] macroscopic constitutive models to represent plastic flow behavior via slip for many materials. In the next two sections of this report, the JC Model, which is of exponential type, and a PL model are considered for the representation of the experimental data.

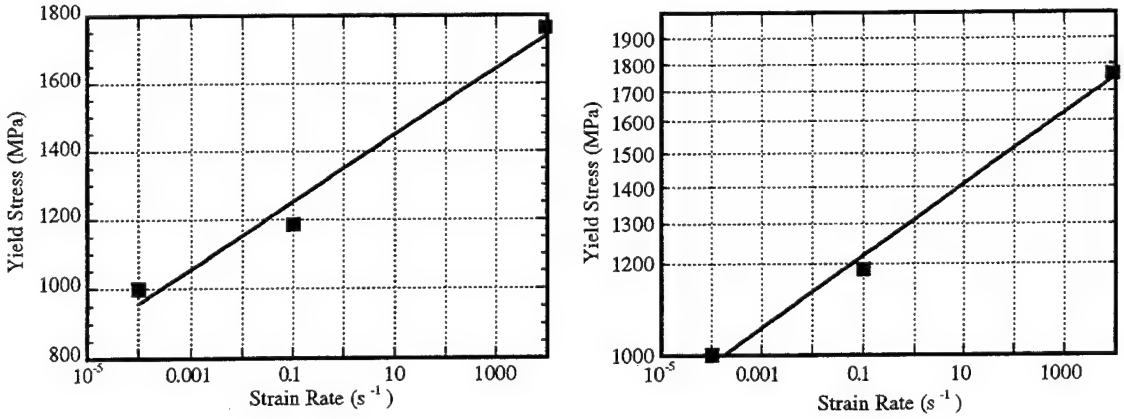

Figure 9. Strain-Rate Sensitivity: (a) Yield Stress vs. Strain-Rate in a Linear-Logarithmic Plot and (b) Yield Stress vs. Strain-Rate in a Logarithmic-Logarithmic Plot.

3.3.2 Johnson-Cook Model.

Johnson and Cook [19] proposed a phenomenological thermo-viscoplastic relationship for flow stress (σ) as a function of plastic strain (ε_p), strain-rate ($\dot{\varepsilon}$), and temperature (T, in Kelvins). This relationship is given by

$$\sigma = \left(\sigma_{yo} + \mathrm{B}\cdot\varepsilon_p^n\right)\cdot\left(1+\mathrm{C}\cdot\ln\left(\frac{\dot{\varepsilon}}{\dot{\varepsilon}_o}\right)\right)\cdot f(\mathrm{T}) \qquad (4)$$

Here, σ_{yo} (=1,186 MPa) is the yield stress at the reference (room) temperature and the reference strain-rate ($\dot{\varepsilon}_o = 0.1\ s^{-1}$). $f(T)$ is defined as $f_o(T) = \left[1 - \left(\frac{T - T_R}{T_M - T_R}\right)^{\alpha}\right]$, where T_M is the melting temperature and T_R is the room temperature. B, C, n, and α are model constants to be determined from the experimental data. Constants B and n are obtained from the stress-strain behavior at the reference strain-rate and temperature. Constant C is obtained from yield stresses at 0.0001 s^{-1} and 9,000 s^{-1}. Yield stress at 9,000 s^{-1} is obtained from extrapolation of the data to the linear elastic response.

To obtain the temperature effects, experiments can be conducted at temperatures lower than the room temperature. In this case, function $f_o(T)$ is not defined. For the model to be valid at lower temperatures, the following functional forms for $f(T)$ have been also proposed in the literature (see Weerasooriya [7] for $f_1(T)$ and Gray et al. [22] for $f_2(T)$):

$$f_1(T) = \left[1 - \left(\frac{T - T_R}{T_M - T_R}\right)\right]^{\alpha} \tag{5}$$

and

$$f_2(T) = \left[1 - \left(\frac{T}{T_R}\right)^{\alpha}\right]. \tag{6}$$

In addition, a function of the Arrhenius form $f_3(T) = \exp\left[\frac{G}{R_g}\cdot\left(\frac{1}{T} - \frac{1}{T_R}\right)\right]$ is considered $f(T)$, where G is a model constant and R_g is the gas constant (R_g = 8.31 J/mol·K). This function is proposed because the plastic deformation by dislocation motion is a thermally activated process [23]. Here, G represents activation energy to overcome the barrier to dislocation glide.

All four functional forms are evaluated using the deformation data at the reference strain-rate ($\dot{\varepsilon}_o$) 0.1 s^{-1} at four tested temperatures: 293, 423, 573, and 732 K. At the reference strain-rate of 0.1 s^{-1}, equation (4) reduces to

$$f(T) = \frac{\sigma}{\left(\sigma_{yo} + B \cdot \varepsilon_p^n\right)}. \tag{7}$$

Figure 10(a)-(d) show the log-log representation of the equation (7) with the respective temperature function indicated in the title of the figure. In these plots, the y axis represents f(T), which is given in Equation (7). Y and x axis variables are chosen for the resultant equation to be linear after rearranging its terms. Using these rearranged equations, stress-strain data at the tested temperatures are plotted for different strains that are indicated in the legends of the plots. Thus, the more linear the data points are represented in the plots, the better the corresponding temperature function. Liner correlation coefficients of the plots for each of the four functional forms are: f_0 -> R = 0.94906, f_1 -> R = 0.96184, f_2 -> R = 0.90499, and f_3 -> R = 0.99189. Therefore, from these plots, it can be seen that the exponential function f_3(T) is the best functional form for f(T). The corresponding JC model constants are

$$\dot{\varepsilon}_o = 0.1\ s^{-1};\ T_R = 293\ K;\ G = 1.81\ kJ/mol;$$

and σ_{yo} = 1,186 MPa; n = 0.6125; B = 1,057 MPa; and C = 0.0227.

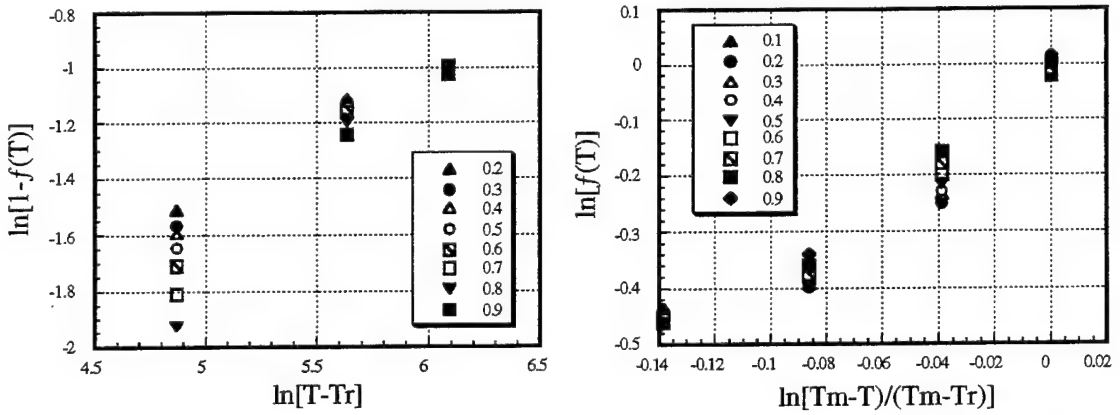

(a). $f_0(T) = [1 - \{(T-Tr)/(Tm-Tr)\}^{\alpha}]$ (b). $f_1(T) = [1 - (T-Tr)/(Tm-Tr)]^{\alpha}$

Figure 10. Evaluation of Different Temperature Functionals for JC Model. Legend of Each Plot Shows the Strain Values.

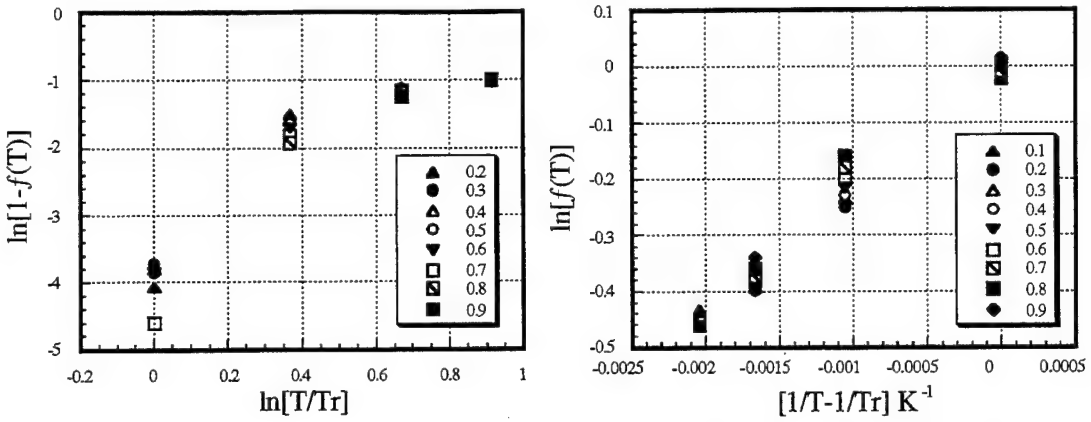

(c). $f_2(T) = [1 - (T/Tr)^{\alpha}]$

(d). $f_3(T) = \exp[k.(1/T-1/Tr)]$

Figure 10. Evaluation of Different Temperature Functionals for JC Model. Legend of Each Plot Shows the Strain Values (continued).

In Figure 11, the comparison between the stress-strain curves generated using this set of constants and the experimental data shows an excellent match.

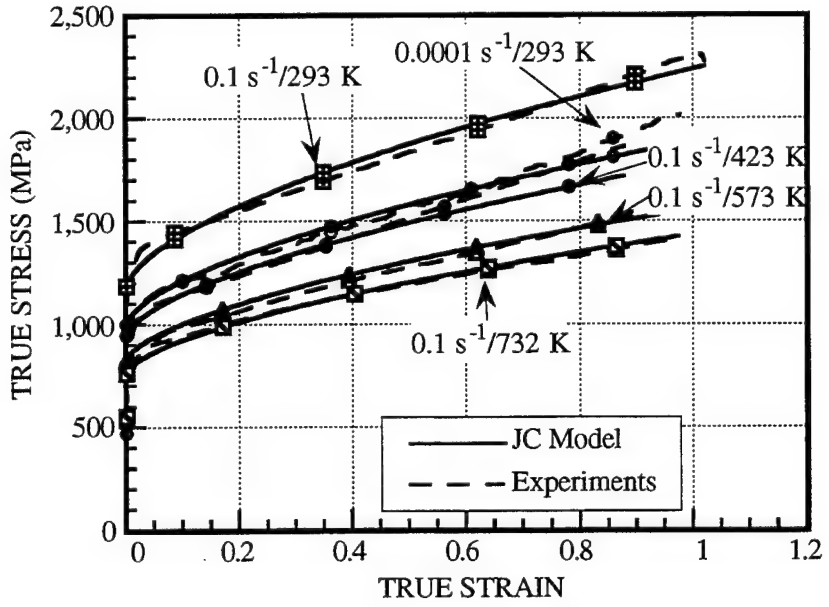

Figure 11. Comparison of JC Model and Experimental Stress-Strain Data Used for Model Calibration.

3.3.3 Power Law Model.

Researchers [20, 21] have proposed a PL relationship for the flow stress (σ) as a function of strain (γ), strain-rate ($\dot{\varepsilon}$), and temperature (T) in the form

$$\sigma = \sigma_o \left(\frac{\varepsilon}{\varepsilon_y}\right)^n \cdot \left(\frac{\dot{\varepsilon}}{\dot{\varepsilon}_o}\right)^m \cdot f(T), \tag{8}$$

where $f(T)$ is given by $f_{oP}(T) = \left(\frac{T}{T_R}\right)^{\alpha}$ to describe the thermo-viscoplastic stress-strain behavior. Here, n, m, and α are model constants to be determined from the experimental stress-strain data. σ_o (= 1,186 MPa) is the yield stress at the reference strain-rate ($\dot{\varepsilon}_o = 0.1\ s^{-1}$) and the reference (room) temperature (T_R = 293 K). The constants ε_y and n are obtained from the room-temperature stress-strain data at 0.1 s^{-1} strain-rate. These two parameters change with the strain and are therefore defined in the form a + b Tanh(ε), where a and b are constants. The strain-rate-hardening exponent m is obtained from the yield stress data at the strain-rates 0.0001 s^{-1} and 9,000 s^{-1}.

Since plastic flow is controlled by dislocation motion that is a thermally activated process, an exponential function of Arrhenius type of the form $f_{1P}(T) = \exp\left[\frac{G}{R_g} \cdot \left(\frac{1}{T} - \frac{1}{T_R}\right)\right]$, where G is the model constant, is also evaluated using 0.1 s^{-1} strain-rate stress-strain data at different temperatures. Results show that both the $f_{\alpha P}(T)$ and $f_{1P}(T)$ functions can correlate the different temperature data reasonably well (for $f_{\alpha P}(T)$: α = -0.4887 with R = 0.9712; for $f_{1P}(T)$: G/R_g = 0.21539 K with R = 0.9787).

Model constants for the PL model with the Arrhenius-type temperature function are

$\dot{\varepsilon}_o = 0.1\ s^{-1}$, T_R = 293 K, σ_o = 1186 MPa, m = 0.02469, and G = 1.79 kJ/mol;

for ε <0.00349, n = 1.0 and ε_y = 0.00349;

and

for $\varepsilon \geq 0.00349$, n = 0.07249 + 0.28874 Tanh(ε) and ε_y = 0.00408 + 0.12381 Tanh(ε).

Figure 12 shows an excellent match between the experimental data and the PL model.

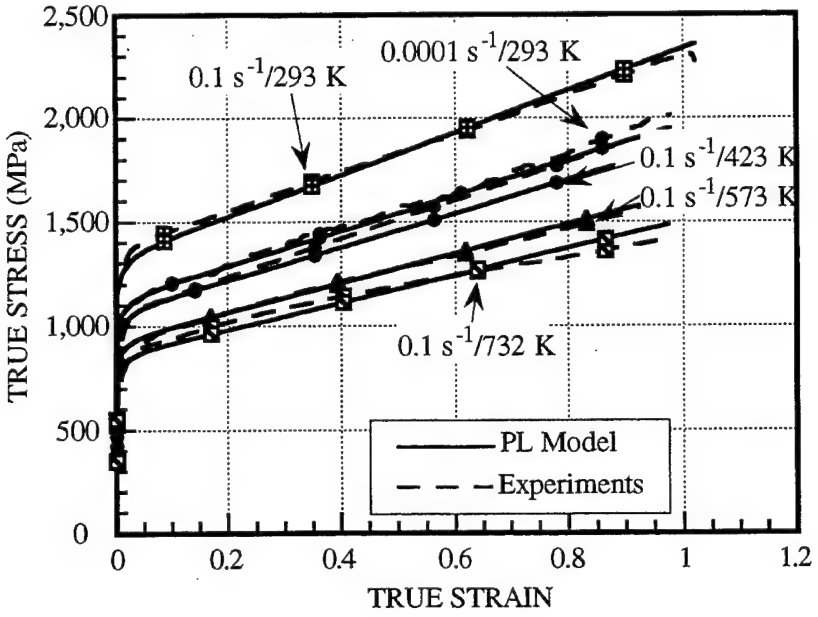

Figure 12. Comparison of PL Model Generated Data and Experimental (Used for Model Calibration) Stress-Strain Data.

3.3.4 Model Predictions of High-Rate Behavior.

In this section, we discuss the ability of the models to predict the experimentally observed high strain-rate (9,000 s^{-1} average strain-rate) stress-strain behavior. Figure 13 shows the experimentally observed stress-strain behavior at 9,000 s^{-1} strain-rate and the adiabatic, as well as isothermal, calculated stress-strain from both models. During computation of the adiabatic stress-strain response, it was assumed that 95% of the plastic work was converted to heat. Temperature increase (ΔT) in the specimen is given by

$$\Delta T = \frac{0.95 W_p}{\rho C_p} \tag{9}$$

where W_p is the plastic work, ρ is the density, and C_p is the specific heat. In addition, the figure shows the calculated temperature of the gauge section under adiabatic conditions as a function of the applied strain using the JC model. Calculated isothermal stress calculated from both models increases with strain. The experiment shows that the material starts to soften with strain just after yielding. This indicates adiabatic heating of the specimen from the start of the plastic

deformation. Material continues to soften through out the test; but, the adiabatic prediction from both models shows strain softening only up to a strain of 0.3. Beyond that, the models show strain hardening. In addition, both models show a lower stress level than that from the experiment up to approximately a strain of 0.45; beyond this strain, stresses predicted by the models are higher than the experimental stress for the same strain. Under adiabatic condition, the calculated temperature of the specimen increases approximately linearly with the strain and reaches a final temperature of 1,190 K. All these calculations assumed a uniform deformation and uniform temperature distribution along the gauge section of the specimen.

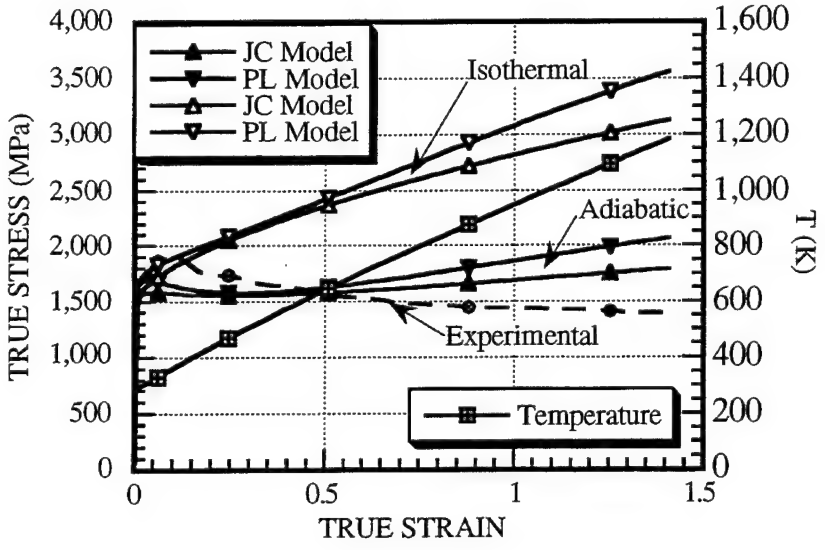

Figure 13. Comparison of JC and PL Model (Adiabatic and Isothermal) Predictions and Experimental Stress-Strain Data at High Strain-Rate (9,000 s^{-1}) of Loading at 293 K. Temperature of the Gauge Area for the Assumed Uniform Adiabatic Deformation (Using JC Model) is Also Given in the Plot.

It can be seen from Figure 9 and work from others that the strain-rate sensitivity increases with strain-rate at higher strain-rates for this alloy [5]. In the two models considered in this paper, strain-rate-sensitivity parameter is a constant and is independent of strain-rate. When the strain-rate-sensitivity parameter of the models is increased to represent the high-rate data from our work and others, the initial stress-strain behavior calculated from the models represents the experimental data well; but, the subsequent calculated hardening and softening behavior does not change. Sensitivity analysis of the parameter G in the temperature functional form shows

that it has to be increased at least by a factor of 2 to obtain a softening response similar to the experimental behavior.

Calculations show that the temperature of the specimen reaches 1,190 K at large strains. Due to the limits of the experimental facility, the highest temperature data that are used for model calibration were obtained at 732 K. Model constants determined with additional stress-strain data that are obtained at temperatures higher than 732 K (up to 1,200 K) may improve the model predictions at larger strains.

Inability to predict the experimental adiabatic stress-strain curve also may indicate that the deformation and the temperature distribution within the specimen may not be uniform due to the possibility of onset of instability at the beginning of strain softening. Although there are no visible signs of localization in the microstructure, it may be necessary to consider that the localization (instability) process starts when the derivative d(stress)/d(strain) ≤ 0. The possibility of nonuniform heating and deformation may require an analysis of the deformation in the compression specimen using a procedure such as a finite element method with adaptive generation of mesh proposed by Batra and Ko [24]. Results of this type of analysis of WHA high-rate compression data will be reported in a future publication.

4. Summary and Conclusions

A set of uniaxial compression experiments was conducted to large strains by systematically varying the strain-rate or the temperature without barreling the specimens. Deformation behavior of the 93W-5Ni-2Fe WHA is obtained at different strain-rates and temperatures. To obtain the effect of loading rates, the tests were conducted at the room temperature at different strain-rates. The range of strain-rates varied from 0.0001 to 9,000 s^{-1}. Tests were also conducted at 0.1 s^{-1} strain-rate at different temperatures to obtain the effect of temperature on deformation behavior. The temperature range was 293 to 732 K. In previous work, we obtained the effect of strain-rate and temperature on the deformation/failure behavior of the same material under torsional loading conditions.

The deformation behavior of this two-phase composite from the present compression and the previous torsion experiments cannot be correlated with the von Mises effective stress-strain criterion, even though this criterion is widely used in most of the computer codes. A

micromechanistic-based methodology such as a crystal plasticity method may be able to better correlate the deformation behavior from these two types of loading for this material.

At high-rate of loading, the torsion specimens fail by localized shear at a much lower shear strain (0.18). Compared to the failure shear strain in torsion, compression specimens do not fail by shear localization to a very large shear strain (2.2). Additional work is necessary to understand this and to formulate failure criteria for this material under multiaxial high-rate loading conditions.

A modified physically based temperature function is proposed for both the PL and the JC models. This proposed function best represents the temperature data for both models compared with the temperature representations found in the literature. The constitutive model constants are obtained for both models with this modified temperature function. The high-rate adiabatic stress-strain curves obtained from these models show the thermal softening only up to a strain of about 0.3. Beyond this strain, stress-strain behaviors from both models show strain hardening. However, experiments show strain softening during all of the plastic deformation. Flow stresses obtained from both models are lower than the experimental flow stress up to about 0.45 strain; beyond this strain, the flow stress from the models is larger than the experimental flow stress. The calculated stress-strain curve from the PL is always higher than that from JC model. It may be necessary to conduct temperature tests at higher temperatures than 732 K (highest temperature from this work) to calibrate these models. The models thus obtained may be able to better predict the high-rate behavior at large strains for WHA. In addition, a more rigorous computation of the adiabatic stress-strain behavior that allows for the nonuniform heating and deformation of the specimen may predict the experimental behavior more closely.

5. References

1. Ekbom, L. "Influence of Microstructure of Liquid-Sintered Tungsten-Base Composites on the Mechanical Properties." *Scandinavian Journal of Metallurgy*, vol. 5, pp. 179–184, 1976.

2. Bose A., and R. M. German. "Sintering Atmosphere Effects on Tensile Properties of Heavy Alloys." *Metallurgical Transaction A*, vol. 19A, p. 2467, 1988.

3. Dowding, R. J. "Tungsten Heavy Alloys: A Tutorial Review." *P/M in Aerospace and Defense Technologies*, p. 109, MPIF, Princeton, NJ, 1991.

4. Weerasooriya, T. and P. A. Beaulieu. "Effects of Strain-Rate on the Deformation and Failure Behavior of 93W-5Ni-2Fe Under Shear Loading." *Material Science and Engineering*, vol. A172 , p. 71, 1993.

5 . Zhou, M., R. J. Clifton, and A. Needleman. "Shear Band Deformation in a W-Ni-Fe Alloy under Plate Impact." *Proceedings of International Conference on Tungsten and Tungsten Alloys - 1992*, p. 343, A. Bose and R. J. Dowding (editors), Metal Powder Industries, 1992.

6. Andrews, E. W., A. F. Bower, and J. Duffy. "Shear Band Formation in a Tungsten Heavy Alloy." *Proceedings of Symposium on Shear Bands and Viscoplastic Theories*, The 29th Annual Technical Meeting of the Society for Engineering Science, La Jolla, CA, September 1992.

7. Weerasooriya, T. "Modeling Flow Behavior of 93W-5Ni-2Fe Tungsten Heavy Alloy." *Proceedings of the Joint AIRAPT/APS Conference on High Pressure Science and Technology*, p. 1021–1024, American Physical Society, CO, July 1993.

8 . Weerasooriya, T. "Modeling Flow Behavior of 93W-5Ni-2Fe Due to Sudden Rate Change." *Proceedings of Shock Compression of Condensed Matter*, p. 319–322, American Physical Society, Seattle, WA, 1995.

9 Weerasooriya, T. "MTL Torsional Split-Hopkinson Bar." MTL-TR-90-27, U.S. Army Materials Technology Laboratory, Watertown, MA, 1990.

10. Kolsky, H. *Stress Waves in Solids*. Oxford University Press, London, 1953.

11. Zukas, J. A., T. Nicholas, H. F. Swift, L. B. Greszczuk, and D. R. Curran. *Impact Dynamics*. John Wiley & Sons, 1982.

12. Semiatin, S. L., G. D. Lahoti, and J. J. Jonas. *Mechanical Testing - Metals Handbook*. Ninth Edition, vol. 8, p. 164, American Society of Metals, 1985.

13. Weerasooriya, T., and R. Swanson. "Experimental Evaluation of the Taylor-Type Polycrystal Model for the Finite Deformation of an FCC Metal (OFHC Copper)." MTL-TR-91-20, U.S. Army Materials Technology Laboratory, Watertown, MA, 1991.

14. Lankford, J., A. Bose, and H. Couque. "High Strain-Rate Behavior of Tungsten Heavy Alloys." *High Strain-Rate Behavior of Refractory Metals and Alloys*, p. 267, R. Asfahani, E. Chen, and A. Crowson (editors), TMS, Warrendale, PA, 1992.

15. Mescall, J., R. Papirno, and J. McLaughlin. "Stress and Deformation States Associated With Upset Tests in Metals." *Compression Testing of Homogeneous Materials and Composites*, ASTM-STP-808, p. 7–23, R Chait and R. Pairno (editors), American Society for Testing and Materials, 1983.

16. Bodner, S. R., and Y. Partom. "Constitutive Equations for Elastic-Viscoplastic Strain Hardening Materials." *ASME Journal Applied Mechanics*, vol. 42, p. 385, 1975.

17. Kocks, U. F., A. S. Argon and M. F. Ashby. "Thermodynamics and Kinetics of Slip." *Progress Material Science*, vol. 19, Pergamon Press, 1975.

18. Follansbee P. S. and U. F. Kocks. "A Constitutive Description of the Deformation of Copper Based on the Use of the Mechanical Threshold Stress as an Internal State Variable." *Acta Metullurgica*, vol. 36, p. 81, 1988.

19. Johnson, G. R. and W. H. Cook. "A Constitutive Model and Data for Metals Subjected to Large Strains, High Strain Rates and High Temperatures." *Proceedings of 7th International Symposium on Ballistics*, p. 541–547, The Hague, The Netherlands, 1983.

20. Costin, L. S., E. E. Crisman, and R. H. Hawley, and J. Duffy. "Mechanical Properties at High Strain-rate." *Proceedings of 2nd Oxford Conference Institute Physics*, p. 90, J. Harding (editor), London, 1980.

21. S. B. Brown, K. H. Kim, and L. Anand. "An Internal Variable Constitutive Model for Hot Working of Metals." *International Journal of Plasticity*, vol. 5, p. 95, 1989.

22. Gray, G. T., S. R. Chen, W. Wright, and M. F. Lopez. "Constitutive Equations for Annealed Metals Under Compression at High Strain-Rates and High-Temperatures." LA-12669-MS, Los Alamos National Laboratory, Los Alamos, NM, January 1994.

23. Frost, H. J., and M. F. Ashby. *Deformation-Mechanism Maps - The Plasticity and Creep of Metals and Ceramics*. Pergamon Press, 1982.

24. Batra, R. C., and K. I. Ko. "Analysis of Shear Bands in Dynamic Axisymmetric Compression of a Thermo-Viscoplastic Cylinder." *International Journal of Engineering Science*, vol. 41, no. 4, p. 529, 1993.

NO. OF COPIES ORGANIZATION

2 DEFENSE TECHNICAL INFORMATION CENTER
DTIC DDA
8725 JOHN J KINGMAN RD
STE 0944
FT BELVOIR VA 22060-6218

1 HQDA
DAMO FDQ
DENNIS SCHMIDT
400 ARMY PENTAGON
WASHINGTON DC 20310-0460

1 DPTY ASSIST SCY FOR R&T
SARD TT F MILTON
RM 3EA79 THE PENTAGON
WASHINGTON DC 20310-0103

1 OSD
OUSD(A&T)/ODDDR&E(R)
R J TREW
THE PENTAGON
WASHINGTON DC 20301-7100

1 CECOM
SP & TRRSTRL COMMCTN DIV
AMSEL RD ST MC M
H SOICHER
FT MONMOUTH NJ 07703-5203

1 PRIN DPTY FOR TCHNLGY HQ
US ARMY MATCOM
AMCDCG T
M FISETTE
5001 EISENHOWER AVE
ALEXANDRIA VA 22333-0001

1 DPTY CG FOR RDE HQ
US ARMY MATCOM
AMCRD
BG BEAUCHAMP
5001 EISENHOWER AVE
ALEXANDRIA VA 22333-0001

1 INST FOR ADVNCD TCHNLGY
THE UNIV OF TEXAS AT AUSTIN
PO BOX 202797
AUSTIN TX 78720-2797

NO. OF COPIES ORGANIZATION

1 GPS JOINT PROG OFC DIR
COL J CLAY
2435 VELA WAY STE 1613
LOS ANGELES AFB CA 90245-5500

3 DARPA
L STOTTS
J PENNELLA
B KASPAR
3701 N FAIRFAX DR
ARLINGTON VA 22203-1714

1 US MILITARY ACADEMY
MATH SCI CTR OF EXCELLENCE
DEPT OF MATHEMATICAL SCI
MDN A MAJ DON ENGEN
THAYER HALL
WEST POINT NY 10996-1786

1 DIRECTOR
US ARMY RESEARCH LAB
AMSRL CS AL TP
2800 POWDER MILL RD
ADELPHI MD 20783-1145

1 DIRECTOR
US ARMY RESEARCH LAB
AMSRL CS AL TA
2800 POWDER MILL RD
ADELPHI MD 20783-1145

3 DIRECTOR
US ARMY RESEARCH LAB
AMSRL CI LL
2800 POWDER MILL RD
ADELPHI MD 20783-1145

ABERDEEN PROVING GROUND

4 DIR USARL
AMSRL CI LP (305)

NO. OF COPIES	ORGANIZATION
1	COMMANDER US ARMY ARDEC G FLEMING PICATINNY ARSENAL NJ 07806-5000
2	COMMANDER US ARMY ARDEC AMSTA AR FSA E E BAKER D KAPOOR PICATINNY ARSENAL NJ 07806-5000
2	SOUTHWEST RSRCH INSTITUTE C ANDERSON J LANKFORD PO DRAWER 28510 SAN ANTONIO TX 78228-0510
1	DIRECTOR LOS ALAMOS NATIONAL LAB MS B296 G T GRAY PO BOX 1663 LOS ALAMOS NM 87545
1	AIR FORCE WRIGHT LAB TECH LIB J FOSTER ARMAMENT DIVISION 101 EGLIN AVE STE 239 EGLIN AFB FL 32542
1	LOS ALAMOS NATIONAL LAB D RABERN GROUP MEE 13 MSJ576 LOS ALAMOS NM 87545
1	LOS ALAMOS NATIONAL LAB TECH LIB PO BOX 1663 LOS ALAMOS NM 87545
1	JOHNS HOPKINS UNIVERSITY DEPT MECH ENGINEERING K RAMESH CHARLES AND 33 ST BALTIMORE MD 21218
1	PENN STATE UNIVERSITY COLLEGE OF ENGINEERING R GERMAN UNIVERSITY PARK PA 16802-6809
1	BROWN UNIVERSITY DIV OF ENGINEERING R CLIFTON PROVIDENCE RI 02912
1	UC SAN DIEGO DEPT APPL MECH AND ENG SVCS R011 S NEMAT-NASSER LA JOLLA CA 92093-0411
1	CALTECH G RAVICHANDRAN MS 105-50 1201 E CALIFORNIA BLVD PASADENA CA 91125
1	INST OF ADVANCE TECH UNIV OF TX AUSTIN S J BLESS 4030 2 W BRAKER LN AUSTIN TX 78759
1	COMMANDER US ARMY RSRCH OFFC K IYER PO BOX 12211 RESEARCH TRIANGLE PARK NC 27709-2211
1	VIRGINIA POLYTECHNIC INST COLLEGE OF ENGNR R BATRA BLACKSBURG VA 24061-0219
1	DIR LLNL D LASILA L170 LIVERMORE CA 94550
	ABERDEEN PROVING GROUND
54	DIR USARL AMSRL WM TD S CHOU A M DIETRICH D DANDEKAR A RAJENDRAN T HADUCH S SCHOENFELD K FRANK M RAFTENBERG J WALTERS T WRIGHT P KINGMAN S SEGLETES

NO. OF COPIES	ORGANIZATION
	T WEERASOORIYA (15 CPS)
	AMSRL WM TC
	W DEROSSET
	T BJERKE
	E KENNEDY
	R MUDD
	W WALTERS
	L MAGNESS
	R COATES
	B SORENSON
	D SCHEFFLER
	K KIMSEY
	AMSRL WM TA
	W GILLICH
	W BRUCHEY
	M BURKINS
	E RAPACKI
	N RUPERT
	J RUNYEON
	W A GOOCH
	G FILBEY
	AMSRL WM MA
	P MOY
	AMSRL WM MC
	R ADLER
	M STAKER
	G KRASKO
	AMSRL WM MD
	R DOWDING
	K CHO
	AMSRL WM MB
	B BURNS
	C HOPPEL
	G GAZONAS

INTENTIONALLY LEFT BLANK

REPORT DOCUMENTATION PAGE

Form Approved
OMB No. 0704-0188

1. AGENCY USE ONLY *(Leave blank)*	2. REPORT DATE	3. REPORT TYPE AND DATES COVERED
	July 1998	Final, 1994 - 1998

4. TITLE AND SUBTITLE
Deformation Behavior of 93W-5Ni-2Fe at Different Rates of Compression Loading and Temperatures

5. FUNDING NUMBERS
1L162618AH80

6. AUTHOR(S)
Tusit Weerasooriya

7. PERFORMING ORGANIZATION NAME(S) AND ADDRESS(ES)
U.S. Army Research Laboratory
ATTN: AMSRL-WM-MF
Aberdeen Proving Ground, MD 21005-5069

8. PERFORMING ORGANIZATION REPORT NUMBER
ARL-TR-1719

9. SPONSORING/MONITORING AGENCY NAMES(S) AND ADDRESS(ES)

10.SPONSORING/MONITORING AGENCY REPORT NUMBER

11. SUPPLEMENTARY NOTES

12a. DISTRIBUTION/AVAILABILITY STATEMENT
Approved for public release; distribution is unlimited.

12b. DISTRIBUTION CODE

13. ABSTRACT ***(Maximum 200 words)***

Low (0.0001 to 0.1 s^{-1}) and high (9,000 s^{-1} average) strain-rate uniaxial compression experiments were performed on a tungsten heavy alloy (WHA) at room temperature; high-rate experiments were conducted using the Compression Split-Hopkinson Bar apparatus. In addition, high-temperature tests at 423, 573, and 732 K were conducted at 0.1 s^{-1} strain-rate. The deformation and failure behaviors of this alloy under compression loading were examined in this report in comparison to the previous torsional work on the same alloy. The deformation behaviors of WHA were modeled using modified Johnson-Cook (JC) and Power-Law (PL) models. A functional form based on microphysics was proposed to represent the temperature part of these models. The model constants were determined from test data at both room and other temperatures. The constants for WHA alloy for these two models are summarized in this report.

14. SUBJECT TERMS
tungsten heavy alloys, high rate loading, compression, constitutive model, high temperature

15. NUMBER OF PAGES
32

16. PRICE CODE

17. SECURITY CLASSIFICATION OF REPORT	18. SECURITY CLASSIFICATION OF THIS PAGE	19. SECURITY CLASSIFICATION OF ABSTRACT	20. LIMITATION OF ABSTRACT
UNCLASSIFIED	UNCLASSIFIED	UNCLASSIFIED	UL

INTENTIONALLY LEFT BLANK.

USER EVALUATION SHEET/CHANGE OF ADDRESS

This Laboratory undertakes a continuing effort to improve the quality of the reports it publishes. Your comments/answers to the items/questions below will aid us in our efforts.

1. ARL Report Number/Author ARL-TR-1719 (Weerasooriya) Date of Report July 1998

2. Date Report Received _____

3. Does this report satisfy a need? (Comment on purpose, related project, or other area of interest for which the report will be used.) _____

4. Specifically, how is the report being used? (Information source, design data, procedure, source of ideas, etc.) _____

5. Has the information in this report led to any quantitative savings as far as man-hours or dollars saved, operating costs avoided, or efficiencies achieved, etc? If so, please elaborate. _____

6. General Comments. What do you think should be changed to improve future reports? (Indicate changes to organization, technical content, format, etc.) _____

CURRENT ADDRESS

_____
Organization

_____
Name E-mail Name

_____
Street or P.O. Box No.

_____
City, State, Zip Code

7. If indicating a Change of Address or Address Correction, please provide the Current or Correct address above and the Old or Incorrect address below.

OLD ADDRESS

_____
Organization

_____
Name

_____
Street or P.O. Box No.

_____
City, State, Zip Code

(Remove this sheet, fold as indicated, tape closed, and mail.)

(DO NOT STAPLE)

DEPARTMENT OF THE ARMY

OFFICIAL BUSINESS

NO POSTAGE
NECESSARY
IF MAILED
IN THE
UNITED STATES

BUSINESS REPLY MAIL
FIRST CLASS PERMIT NO 0001,APG,MD

POSTAGE WILL BE PAID BY ADDRESSEE

DIRECTOR
US ARMY RESEARCH LABORATORY
ATTN AMSRL WM TD
ABERDEEN PROVING GROUND MD 21005-5066